Supporting Information

Long Range Distance Measurements in Proteins at Physiological Temperatures Using Saturation Recovery EPR Spectroscopy

Zhongyu Yang,[1] Gonzalo Jiménez-Osés,[2] Carlos J. López,[1] Michael D. Bridges,[3] K. N. Houk,[2] and Wayne L. Hubbell[1]

1. Jules Stein Eye Institute and Department of Chemistry and Biochemistry, University of California, Los Angeles, CA 90095, United States
2. Department of Chemistry and Biochemistry, University of California, Los Angeles, CA 90095, United States
3. Current address: Department of Chemistry and Biochemistry, California State University, Fullerton, CA 92831

1. Experimental Details.

T4L sample preparation. All DNA used in this work were generated by QuikChange site-directed mutagenesis (Agilent QuikChange) of the pET11a-T4L genetic construct.[1] Mutations were verified by DNA sequencing. All mutants contain the pseudo-wild-type mutations C54T and C97A.[2] All mutants of T4L were expressed, purified, and then desalted (to remove dithiothreitol, DTT) into a buffer suitable for spin labeling (the "spin labeling buffer", which contains 50 mM MOPS buffer and 25 mM NaCl at pH 6.8) using a previously reported procedure.[3] Labeling with R1, R1p, and RX spin probes was performed as reported previously.[3,4] Excess spin label was removed using an Amicon spin concentrator (Millipore, 10,000 MWCO, 50 ml). Samples immobilized on CNBr activated sepharose were prepared using the procedure described previously.[1]

Far UV CD spectroscopy. Samples for Far UV CD analysis were prepared in buffer consisting of 50 mM MOPS, 25 mM NaCl at pH 6.8. Typical protein concentrations were ~ 0.50 mg/ml. The spectra were recorded in the wavelength range of 200-260 nm using the following set of parameters: scan speed = 50 nm/min, data integration time = 0.25 seconds, standard sensitivity, data pitch = 0.4 nm, bandwidth = 2 nm, and continuous scanning mode. The spectra shown are averages of 9 accumulations. Data showing a photomultiplier tube voltage exceeding 600 V was truncated (200-206 nm). The baseline corrected raw ellipticity in millidegrees was converted to mean residue ellipticity ([Θ]) in units of deg*cm^2*dmol^{-1} using the following equation:[5,6]

$$[\theta] = \frac{\theta * \frac{MW}{pb}}{l * C * 10\ dmol}$$

where θ is ellipticity, MW is the molecular weight (17.4 kDa), #pb is the number of peptide bonds (# amino acids -1), l is the path length in cm, and C is the protein concentration in mg/ml.

Room Temperature SR. The SR was carried out using a Bruker E580 spectrometer equipped with a loop-gap resonator and a Stanford signal amplifier as described before.[7] The experimental temperature was controlled using a Bruker temperature controller. Each sample with a typical volume of 2-3 μl was loaded into a TPX capillary with an inner diameter of 0.6 mm (Molecular Specialties Inc., Milwaukee, WI). Before each measurement, the sample was equilibrated at 298 K under nitrogen flow to remove oxygen. The saturating pulse length was 1 μs, with an incident power of 250 mW. The observing power was 100 μW. Both the saturating and observing pulses were set to the maximum absorbance of the nitroxide absorbance spectrum. A shot repetition time (SRT) of 45 - 48 μs was used for each data acquisition. The number of points in each curve was 2048 with a step size of 20 ns. The total number of acquisitions was 2.1 million. ***Typical signal acquisition time is ~5-6 min for trace.***

Low Temperature SR. Each low temperature sample (SR and DEER) contained ~ 25% (v/v) glycerol as a cryoprotectant. A sample with the volume of 12–16 μl was loaded into a borosilicate capillary with an inner

diameter of 1.2 mm (Vitroglass). Prior to measurement, the sample was flash-frozen using liquid nitrogen. The pulse sequence used was π/2 -t1- π/2-t1- π/2-tp- π /2-t2- π - echo, where the π /2 pulse length was adjusted to be 6-8 ns, and the intervals of t1 and t2 were 40 ns and 200 ns, respectively. The first three π /2 pulses serve as the saturating pulse train. The last two pulses serves as the (echo-based) detection pulses.[8] All pulses were set to the maximum absorbance of the nitroxide absorbance spectrum. The interval, tp, was stepped out by 2 μs with a total of 512 points. The SRT used in all LT SR experiments was 1.5 ms. Typical signal averaging time for each LT SR data was 20-30 mins.

Field-Swept Electron-Spin Echo (FS-ESE) and ESEEM spectroscopy. The FS-ESE and ESEEM experiments were carried out using a MS2 resonator with a TWT signal amplifier as in the LT SR experiments. The experimental temperature (20 K) was controlled using an Oxford temperature controller and liquid helium. Similar sample volume was used as in LT SR experiments. For the FS-ESE experiment, the standard Hahn echo pulse sequence π/2-t1-π-t1-echo was used, where the π/2 pulse length was adjusted to be 16 ns, and the intervals of t1 was 200 ns. The SRT used in FS-ESE experiments was 1.5 ms. Typical signal averaging time is ~ 10 min for each sample. For the 3 pulse ESEEM experiment, the pulse sequence was π/2-t1-π/2-t2- π/2-t1-stimulated echo, where the π/2 pulse length was adjusted to be 16 ns, and the t1 was 200 ns. The interval t2 was incremented from 400 ns with a step size of 16 ns, for a total of 1,024 points. Same SRT (1.5 ms) was used for ESEEM experiment. A four-step phase cycle was employed to eliminate unwanted signals.[9,10] Typical signal averaging time is ~20 min for each sample.

2. Details of QM calculations

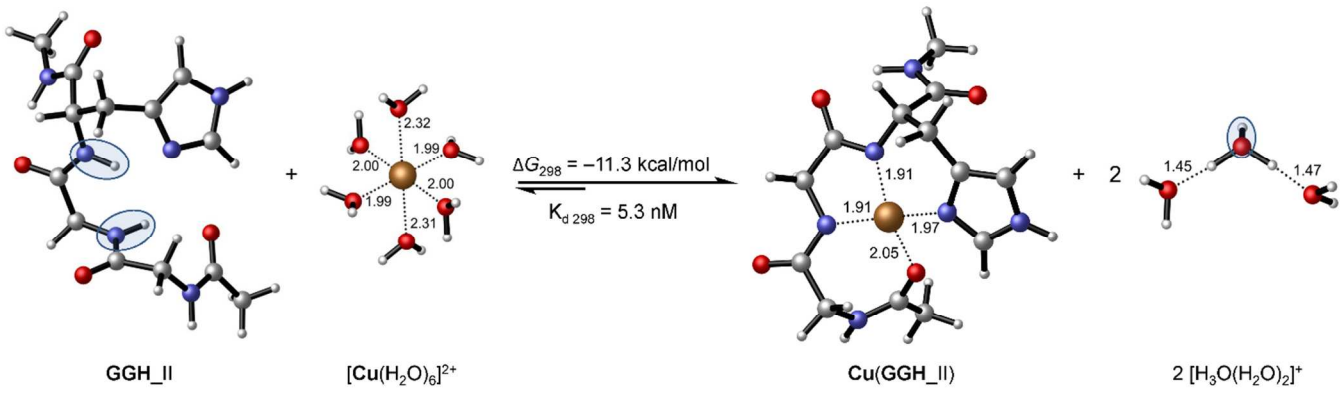

Figure S1. Binding of Cu^{2+} to the Gly-Gly-His motif. Deprotonation of two backbone amides and desolvation of the metal center in necessary to achieve coordination. The equilibrium is shifted towards the formation of the copper(II) chelate, which dissociation constant at room temperature ($K_{d\ 298}$) is calculated to be in the nM range.

Table S1. SMD(H_2O)/B3LYP/6-311+G(d,p) // B3LYP/6-31G(d) absolute energies, enthalpies, free energies, entropies and lowest frequencies of the structures considered in this work.

Structure	E_{elec} (Hartree)[a]	E_{elec} + ZPE (Hartree)[a]	E (Hartree)[a]	H (Hartree)[b]	S (cal mol^{-1} K^{-1})[b]	G (Hartree)[b]	Lowest freq. (cm^{-1})
Cu(GGH_Ia)	–2776.155209	–2775.838949	–2775.815441	–2775.814497	166.3	–2775.889357	29.0
Cu(GGH_Ib)	–2776.155955	–2775.839904	–2775.816322	–2775.815378	167.5	–2775.890340	26.1
Cu(GGH_II)	–2776.637128	–2776.306337	–2776.282523	–2776.281579	168.2	–2776.357161	22.0
GGH_II	–1137.293816	–1136.940804	–1136.916954	–1136.916010	171.3	–1136.990987	20.2
$[Cu(OH_2)_6]^{2+}$	–2099.068258	–2098.918253	–2098.901070	–2098.900126	130.0	–2098.959810	28.0
$[H_3O(H_2O)_2]^{+}$	–229.859219	–229.775958	–229.768494	–229.767550	81.5	–229.805815	68.7

[a] 1 Hartree = 627.51 kcal mol^{-1}. [b] Thermal corrections at 298.15 K.

Cartesian coordinates of the structures optimized through QM calculations

Structure Cu(GGH_Ia) [B3LYP/6-31G(d)]

C	-2.67007600	-2.01206600	-0.45088900
C	-3.39498300	-0.69276800	-0.10930600
C	-0.41356400	-2.86217300	-0.83448800
C	2.37159000	-0.32922000	-0.69939300
C	3.72411200	-1.37931100	2.68281200
C	2.34873900	0.97166000	-1.52223700
C	1.35900600	2.02992100	-1.13221000
C	1.00199400	-2.28766500	-0.67554800
C	-0.58141200	2.90653500	-0.65894900
C	1.52317400	3.39104000	-1.14044700
C	2.99031600	-0.12407400	0.69723900
H	3.93785700	-0.36165200	3.01677300
H	4.63812300	-1.98299300	2.76292200
H	2.13477300	0.67736500	-2.55926800
H	3.34891400	1.41851100	-1.51101600
H	-1.62105800	3.01813600	-0.39223700
H	0.06523400	4.91165000	-0.73967500
H	2.39160300	4.00686800	-1.31522100
H	-4.17284500	-0.89453500	0.63274000
H	-3.91587400	-0.33488700	-1.01449300
H	-0.57768200	-3.62819700	-0.06219100
H	-0.43971900	-3.40002600	-1.79752300
H	3.04229400	-1.02547800	-1.22635800
H	2.96546900	-2.15036900	0.81450600
H	2.96426500	-1.81742800	3.34465300
N	-2.43899000	0.30198100	0.39759100
N	0.03564500	1.75141700	-0.82610300
N	0.28239100	3.93205900	-0.84389000
N	-1.37767200	-1.79289200	-0.75680000
N	1.05112100	-0.94065300	-0.63699300
N	3.26332300	-1.30620700	1.31462700
O	-3.25549400	-3.10495900	-0.44038600
O	1.99406200	-3.05317100	-0.60276100
O	3.22495000	0.98477300	1.18345800
C	-2.89995500	1.09728800	1.38342900
O	-4.08675500	1.20359300	1.74805800
C	-1.84716300	1.89245000	2.17012300

H	-1.90057500	1.56391400	3.21478400
H	-0.82210400	1.75382800	1.81781300
H	-2.09546400	2.96195700	2.16769600
Cu	-0.68064500	-0.07545500	-0.38140400

Structure Cu(GGH_Ib) [B3LYP/6-31G(d)]

C	-2.91667100	-1.65563800	-0.20744300
C	-3.43226900	-0.22747100	0.02147500
C	-0.90086600	-2.92463200	-0.59201500
C	2.32781000	-1.03064300	-0.29184800
C	2.51563400	-0.12667600	3.40844900
C	2.59939300	-0.08408500	-1.48213800
C	1.93727400	1.25161200	-1.33776300
C	0.60590200	-2.65987000	-0.50696800
C	0.38683100	2.70755300	-0.82850100
C	2.46364900	2.49169300	-1.58048600
C	2.92626600	-0.44346700	0.99758900
H	3.50984400	0.31782300	3.32248300
H	2.55156000	-0.94662700	4.13851800
H	2.24266900	-0.59444400	-2.38617500
H	3.67805600	0.07047600	-1.58417100
H	-0.52152500	3.12467000	-0.39889300
H	1.54280100	4.40492400	-1.27875400
H	3.44044900	2.79868300	-1.92081400
H	-4.09952300	-0.28621600	0.89159000
H	-4.07481000	0.03468800	-0.83787100
H	-1.19922500	-3.60618000	0.21990600
H	-1.08184700	-3.47928200	-1.52547800
H	2.88373300	-1.96027800	-0.48101300
H	1.22922600	-1.00315600	1.91893700
H	1.81326100	0.63341400	3.77453600
N	-2.34293600	0.73651600	0.20776000
N	0.63411500	1.40739900	-0.87504600
N	1.46632900	3.39954400	-1.26205800
N	-1.61974100	-1.67521100	-0.53740100
N	0.91756000	-1.36478200	-0.19958800
N	2.14347000	-0.60196800	2.09679000
O	-3.67996100	-2.62831500	-0.08890400
O	1.41469400	-3.57577400	-0.71927200
O	4.04035500	0.08552300	1.01859700
C	-2.64757200	1.94161700	0.70502700
O	-1.81372400	2.85381100	0.93141300
C	-4.11345600	2.26765300	1.04866500
H	-4.16505600	3.32088200	1.33227500
H	-4.79028200	2.08207900	0.20576300
H	-4.47526400	1.65799500	1.88630900
Cu	-0.58890000	-0.09682000	-0.29480300

Structure Cu(GGH_II) [B3LYP/6-31G(d)]

C	-3.02042500	-1.40651500	-0.74009000
C	-3.75471400	-0.04662800	-0.74067100
N	-1.69313200	-1.30958400	-0.56945900
O	-3.68519200	-2.44250900	-0.85894800
H	-4.74703600	-0.18678000	-1.17058400
H	-3.21635400	0.71238300	-1.31525400
N	-3.92819700	0.46348400	0.62383800
C	-0.95681300	-2.56698100	-0.52527200
Cu	-0.56714300	0.21440800	-0.34253700
C	-2.95588200	1.07020400	1.31050700
H	-4.76022000	0.18071000	1.12399400
C	0.54596800	-2.31347200	-0.51140000
H	-1.22263400	-3.16549700	0.35772500
H	-1.19099000	-3.19919600	-1.39191900
N	0.88844200	-1.00748200	-0.56200500
N	0.53049900	1.82838700	-0.60403800
O	-1.83695000	1.33363700	0.80844800
C	-3.24467900	1.46810200	2.73876100
O	1.34731400	-3.26648500	-0.46087400

C	2.29961000	-0.69678600	-0.77875300
C	1.83268500	1.80482400	-1.08204800
C	0.28538900	3.06322400	-0.18872400
H	-3.02119600	2.53148400	2.86576100
H	-4.27966600	1.28177500	3.03816900
H	-2.57441500	0.91170700	3.40231500
C	2.45709200	0.56590000	-1.64221800
C	3.08700700	-0.59100900	0.54660000
H	2.73690600	-1.53331200	-1.34137800
C	2.35810700	3.06261400	-0.96252100
H	-0.63243200	3.39559700	0.26855100
N	1.36600500	3.84353300	-0.39811300
H	2.00952000	0.34633300	-2.62086000
H	3.52169700	0.75875000	-1.80543800
N	3.20635100	-1.78569900	1.17990200
O	3.55843300	0.46961200	0.96060300
H	3.33800000	3.45074300	-1.18989500
H	1.44404900	4.81957700	-0.15239800
C	3.83949600	-1.92509600	2.47521400
H	2.72204200	-2.57710800	0.75011600
H	4.30008600	-0.96852100	2.72862400
H	4.61271600	-2.70220000	2.45050600
H	3.11140200	-2.18708200	3.25450200

Structure GGH_II [B3LYP/6-31G(d)]

C	-2.22949500	-1.46147600	-1.02803800
C	-3.15657600	-0.25052800	-1.23117500
N	-1.57429100	-1.47656900	0.17235700
O	-2.08563900	-2.31435500	-1.89357100
H	-3.59450700	-0.34873300	-2.22532100
H	-2.54775400	0.65908000	-1.19189000
N	-4.23740400	-0.13322400	-0.25572800
C	-0.56772200	-2.47803300	0.46206000
C	-4.07724800	0.44571400	0.96256200
H	-5.12473400	-0.55917600	-0.48139200
C	0.87521400	-2.12175000	0.06431200
H	-0.56862600	-2.70922000	1.53255200
H	-0.82230100	-3.39262600	-0.07794600
N	1.08200900	-0.84912500	-0.32322300
N	-0.13483300	1.75377700	-0.68376300
O	-2.98812100	0.88336700	1.34594600
C	-5.31737800	0.52875600	1.83479200
O	1.75968400	-2.98233500	0.14686300
C	2.32122200	-0.33152300	-0.90967100
C	1.20801200	1.95716200	-0.97453800
C	-0.50785000	2.77585200	0.05964000
H	-5.50266700	1.57882000	2.08115600
H	-6.21427300	0.11058900	1.36820500
H	-5.12509500	0.00303400	2.77510400
C	1.99089800	0.92916400	-1.73998300
C	3.44134900	-0.03127400	0.12749500
H	2.71774000	-1.10759900	-1.57878400
C	1.63160500	3.12561800	-0.39450600
H	-1.48830900	2.91046600	0.49461500
N	0.52596000	3.64121600	0.25286700
H	1.41430000	0.61587200	-2.61804200
H	2.93304800	1.35908000	-2.08471200
N	3.73849400	-1.07572000	0.93799100
O	4.02316100	1.05242700	0.15098400
H	2.60281800	3.59213600	-0.35174000
H	0.49611400	4.49657600	0.78840300
C	4.78485000	-1.01056800	1.94025000
H	3.23359800	-1.94959700	0.78316400
H	5.16870900	0.01043400	1.96181800
H	5.60855100	-1.69507100	1.70110500
H	4.39370400	-1.27162500	2.93088000
H	0.28556000	-0.21410400	-0.34880000
H	-1.71938500	-0.68634700	0.79712700

Structure [Cu(OH2)6]2+ [B3LYP/6-31G(d)]

Cu	3.45210700	3.61300100	-0.00011400
O	1.94856100	2.42741000	-0.56275300
H	1.14543400	2.56114900	-0.02565400
H	1.69594200	2.07132000	-1.43338500
O	2.62052100	5.24630400	-0.77100900
H	3.14706900	6.06596200	-0.78957500
H	1.99329600	5.28103800	-1.51525300
O	1.88942100	3.91391200	1.68139900
H	1.42334400	4.76692700	1.73048300
H	1.81499600	3.53530400	2.57529700
O	4.95555700	4.79861700	0.56289700
H	5.75877500	4.66505300	0.02589300
H	5.20801300	5.15462000	1.43361300
O	4.28373200	1.97972000	0.77082000
H	3.75713300	1.16009300	0.78947000
H	4.91088100	1.94505700	1.51513300
O	5.01456400	3.31213700	-1.68147500
H	5.48060800	2.45910200	-1.73049700
H	5.08934800	3.69087500	-2.57528900

Structure [H3O(H2O)2]+ [B3LYP/6-31G(d)]

O	2.09595200	-0.47379600	0.01137000
H	2.68094600	-0.39415700	0.78387500
H	2.67215400	-0.54572800	-0.76787200
O	-0.00480600	0.90687400	0.06843300
H	-0.05131800	1.61708600	-0.59831800
H	0.89439700	0.36746400	-0.00228400
H	-0.87303600	0.30591300	0.02634700
H	-2.17033200	-1.34043200	-0.29892900
H	-2.76943900	-0.27561500	0.67290700
O	-2.13906800	-0.39989400	-0.05676900

3. FS-ESE and ESEEM spectra.

FS-ESE spectroscopy was employed to confirm presence of both Cu^{2+} and nitroxide spins, as well as investigate Cu^{2+} binding geometry. As shown in Fig. S2 (left), in each Cu^{2+} bound samples, FS-ESE reports spin echo intensity for both the Cu^{2+} and the nitroxide spin label. Furthermore, as shown in Fig. S2 (left), the $A_{\|}$ values of the Cu^{2+} spectral region for all the three samples were found to be ~165 G, consistent with the 3N1O planar square binding motif.[11]

ESEEM spectroscopy was employed to identify nuclei that are interacting with the electron spin. The ESEEM spectra on three examined samples show three sharp peaks below 2 MHz, 1 broad peak at ~4 MHz (the double quantum transition), and 1 peak at 14.8 MHz (proton ESEEM), which are well-known to be characteristic signal from interaction of Cu^{2+} electron spin with the distant nitrogen on a histidine residue.[12]

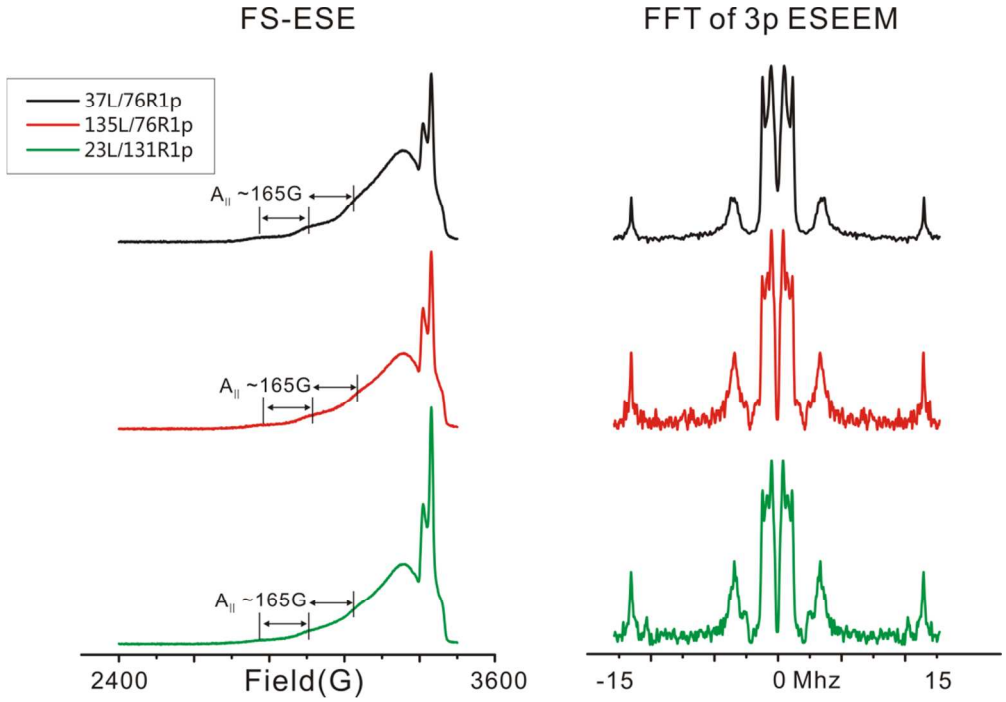

Figure S2. FS-ESE (left) and 3 pulse ESEEM spectra (right) of the three loop-containing samples.

4. Additional data for molecular motional effects on distance measurements.

Similar to data presented in Fig. 6 of the main text, when proteins are in buffer at 298 K the calculation of distance using the fast motional limit agrees well with the "DEER averaged" distance, while in the presence of 30 % (w/v) Sucrose, the rigid limit is a more appropriate theory to calculate the distances (Fig. S3).

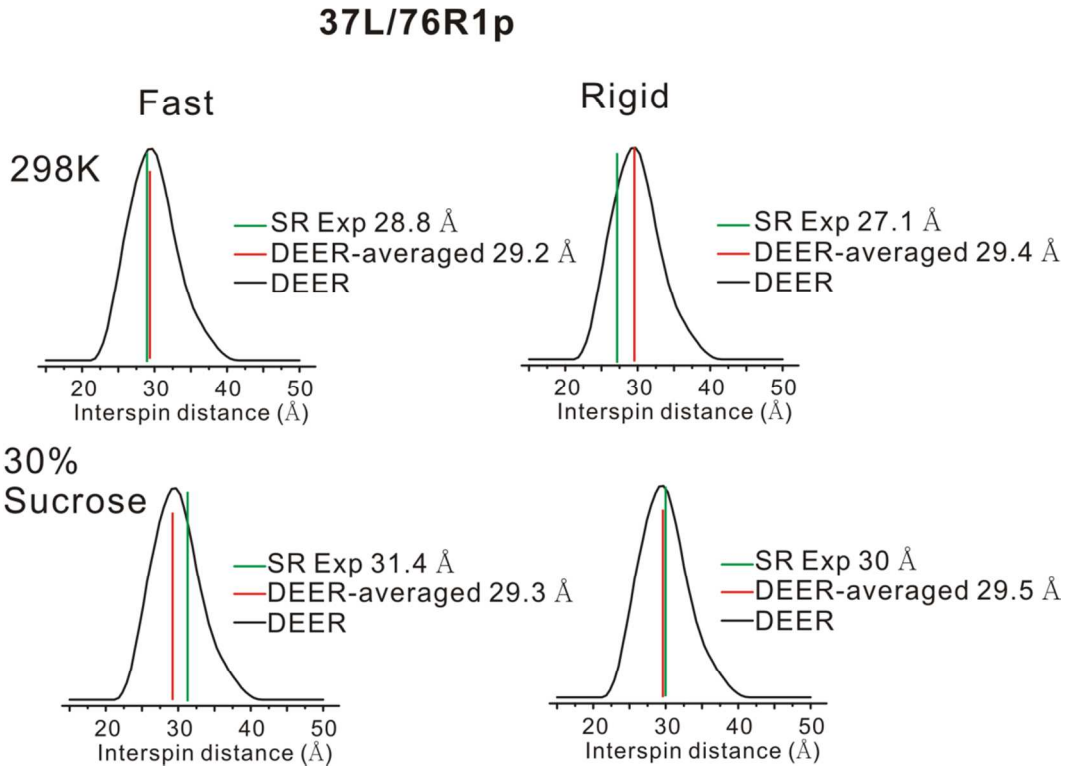

Figure S3. Effects of molecular rotational motion on distance measurements of the 37L/76R1p mutant. Two different conditions were investigated, namely protein in buffer at 298K, and protein in 30 % (w/v) sucrose at 298 K. For each row, two theories, the fast motional limit (the "Fast" columns) and the rigid limit (the "Rigid" column), were used to calculate the average Cu^{2+}-R1p distances based on distance distribution obtained from DEER experiments. Green bars represent the average Cu^{2+}-nitroxide distance obtained from SR experiments, red bars illustrate the "DEER averaged" distance using the corresponding approximation, and grey curves are the Cu^{2+}-nitroxide distance distribution obtained from DEER.

5. Calculation of distances using the fast motional limit and the rigid limit.

To calculate the Cu^{2+}-nitroxide distance using the fast motional limit, Equation 1 was programed into an excel file, which computes the r based on inputs of T_{1s} and T_{1s}^{0}. The constants used in the excel program are: h=6.626e-34 J s, g_s=2.0061, g_f=2.1166, β_e=9.27e-24 J/T, T_{1f}=T_{2f}=3 ns, ω_s=58.6 GHz rad, ω_f=61.9 GHz rad.[13]

Under the rigid limit, a home built LabView based program was used to perform integration over the θ angle as shown in Equation 2 of the main text. At 298 K, the same set of constants was used as in the fast motional limit. At 110 K, a T_{1f} and a T_{2f} of 250 ns were used based on Sarver *et al*.[8]

6. **Table S2. Comparison of Cu^{2+}-nitroxide distances obtained from RT SR and LT SR.**

Sample Name	Experimental Cu^{2+}-spin label distance from RT SR	Experimental Cu^{2+}-spin label distance from LT SR
23L/131R1p	32.0 Å	31.3 Å
37L/76R1p	28.8 Å	29.5 Å
135L/76R1p	30.0 Å	28.3 Å
135L/61RX65	36.0 Å	34.0 Å

7. **Modeling of the "open" and the "closed" states of T4 lysozyme with the Cu^{2+} center and R1p.**

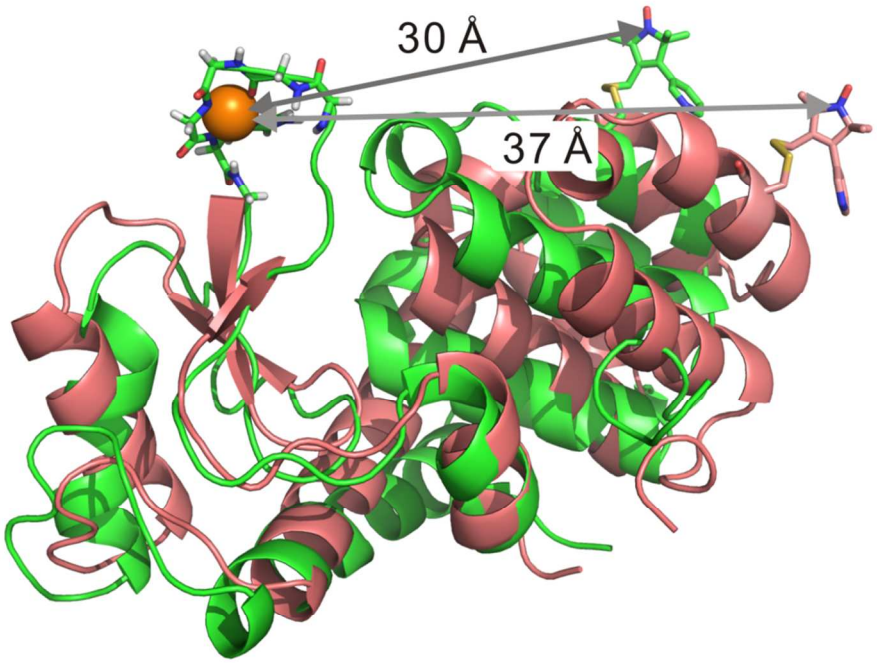

Figure S4. Structural models of the "open" (pink) and the "closed" (green) states of T4 lysozyme, using reported pdb files of 150L and 3LZM, respectively.[2] On each structure, the Cu^{2+} center (brown sphere) was inserted in between residues 23 and 24 based on the MD simulation, and the R1p structure was attached to residue 131 based on a reported crystal structure of an analogous spin label (pdb file: 1ZUR). The two structural models are aligned with Cu^{2+} bound center. The distance between the Cu^{2+} and the R1p spin label are found to be 30 and 37 Å for the "closed" and the "open" state of T4L, respectively. This 7 Å difference in

Cu^{2+}-nitroxide distance is close to the 7 Å splitting in distance distribution reported in Figure 6 of the main text.

8. RT SR data with fitting and residual signal

This section provides the raw data of RT SR for all samples used in this study with corresponding conditions (see subtitle of each figure). For all curves, a single exponential function was used to fit the time domain recovery signal; the resultant featureless residual signal indicate near 100 % occupation of Cu^{2+} binding site for each sample.

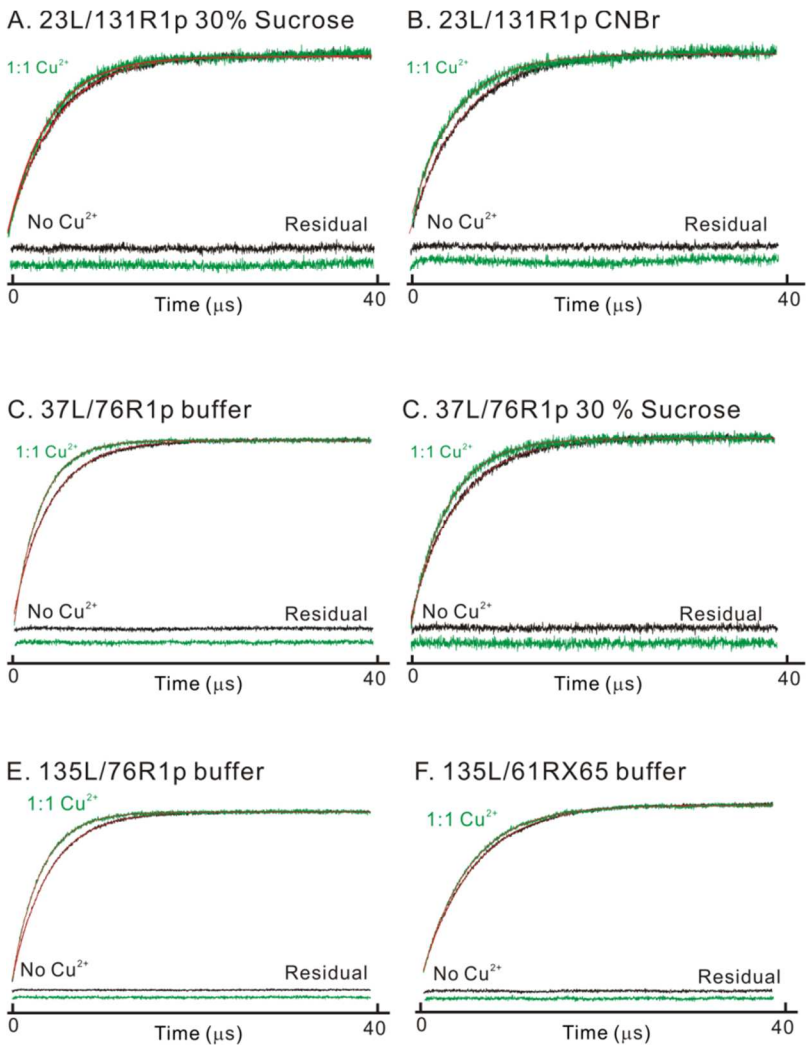

Figure S5. The raw RT SR data with fits and residual signal for samples used in this study. Sample names and experimental conditions are indicated by the subtitle. For each sample, the SR signal in the absence (black) and presence (green) of Cu^{2+} were fit to a single exponential function (red). The residual after fit are listed below the actual data. Black and green residuals are from fits to data in the absence (black) and presence (green) of Cu^{2+}, respectively.

9. Table S3. Apparent T1s from SR data using single exponential fitting.

Sample + condition	T_{1s}^0 (μs)	T_1s (μs)
23L/131R1p 298K	3.9	3.2
23L/131R1p 308K	3.6	3.0
23L/131R1p 30 % Sucrose	5.2	4.2
23L/131R1p CNBr-Sepharose	5.9	4.7
23L/131R1p 110K	**355**	**283**
37L/76R1p 298K	4.0	2.8
37L/76R1p 308K	3.5	2.6
37L/76R1p 30 % Sucrose	5.0	3.8
37L/76R1p 110K	**361**	**267**
135L/76R1p 298K	3.9	3.0
135L/76R1p 110K	**361**	**249**
135L/61RX65 298K	5.8	5.0
135L/61RX65 110K	**361**	**245**

10. Uncertainties in distance measurement using RE.

Each SR experiment was repeated 3 times, in order to obtain the uncertainty in measurement. For RT SR, the uncertainty in each T_1 reported is in the range of 50 -100 ns. The uncertainty in distance calculation is therefore in the range of 0.5 to 1 Å. For LT SR, the uncertainty in each T_1 reported is in the range of 5 - 10 μs. The uncertainty in distance calculation is in the range of 1 to 2 Å.

11. Raw data and fitting for LT SR

This section provides the raw data of LT SR for all samples used in this study. For all curves, a single exponential function is used to fit the data.

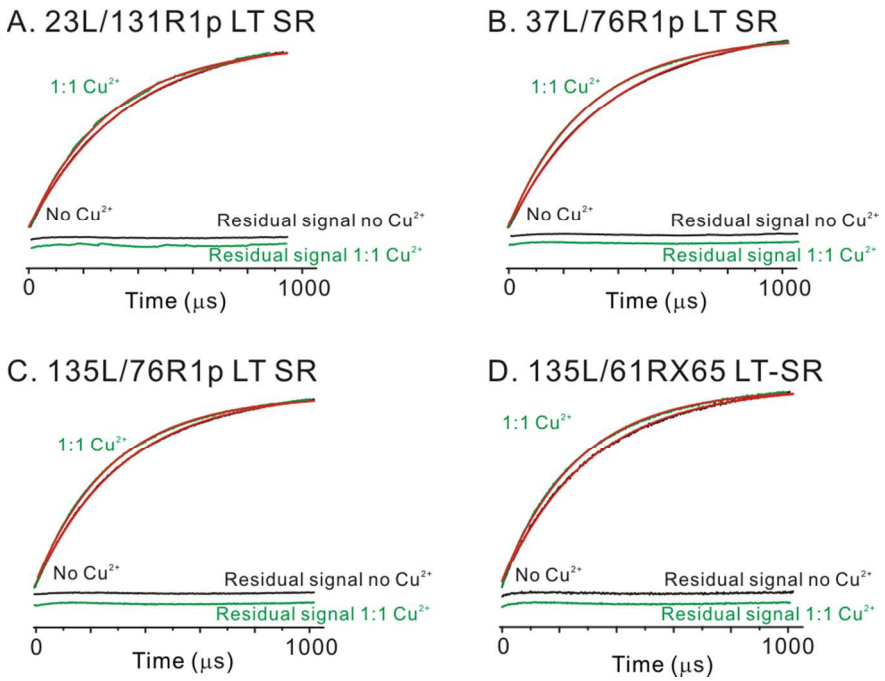

Figure S6. The raw LT SR data in the absence (black) and presence (green) of Cu^{2+}. Fit to each data set using a single exponential function are shown in red. The corresponding residuals after fitting are shown below each trace.

12. Cu^{2+}-nitroxide DEER at 20 K.

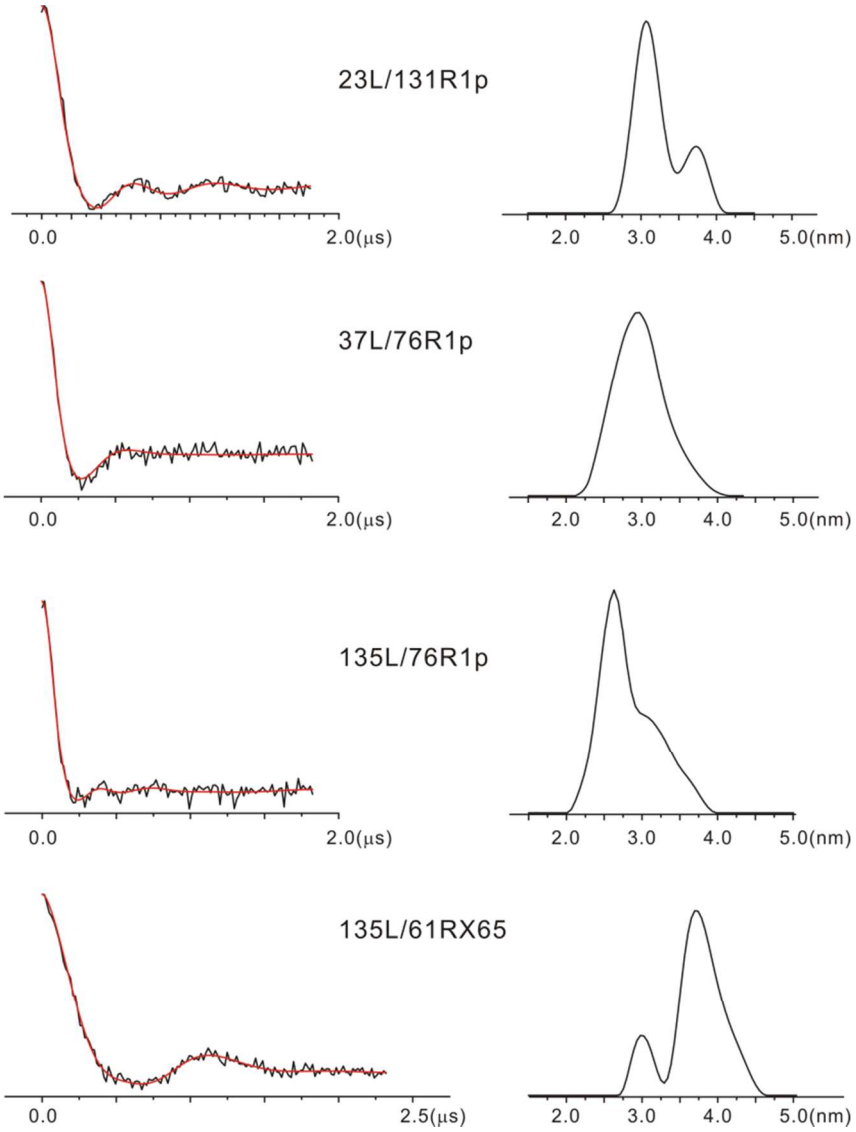

Figure S7. (Left) Baseline corrected DEER data (black) with fitting (red) using LongDistances.[6] (Right) The distance distribution obtained from LongDistances for each sample.

References:

(1) López, C. J.; Fleissner, M. R.; Guo, Z.; Kusnetzow, A. K.; Hubbell, W. L. *Protein Sci.* **2009**, *18*, 1637.

(2) Matsumura, M.; Wozniak, J. A.; Sun, D. P.; Matthews, B. W. *J. Biol. Chem.* **1989**, *264*, 16059.

(3) Fleissner, M. R.; Bridges, M. D.; Brooks, E. K.; Cascio, D.; Kálai, T.; Hideg, K.; Hubbell, W. L. *Proc. Natl. Acad. Sci. U. S. A.* **2011**, *108*, 16241.

(4) Fawzi, N.; Fleissner, M.; Anthis, N.; Kálai, T.; Hideg, K.; Hubbell, W.; Clore, G. M. *J. Biomol. NMR* **2011**, *51*, 105.

(5) Greenfield, N. J.; Fasman, G. D. *Biochemistry* **1969**, *8*, 4108.

(6) Chen, Y.-H.; Yang, J. T. *Biochem. Biophys. Res. Comm.* **1971**, *44*, 1285.

(7) Bridges, M.; Hideg, K.; Hubbell, W. *App. Magn. Reson.* **2010**, *37*, 363.

(8) Sarver, J.; Silva, K. I.; Saxena, S. *App. Magn. Reson.* **2013**, *44*, 583.

(9) Fauth, J. M.; Schweiger, A.; Braunschweiler, L.; Forrer, J.; Ernst, R. R. *J. Magn. Reson. (1969)* **1986**, *66*, 74.

(10) Gemperle, C.; Aebli, G.; Schweiger, A.; Ernst, R. R. *J. Magn. Reson. (1969)* **1990**, *88*, 241.

(11) Aronoff-Spencer, E.; Burns, C. S.; Avdievich, N. I.; Gerfen, G. J.; Peisach, J.; Antholine, W. E.; Ball, H. L.; Cohen, F. E.; Prusiner, S. B.; Millhauser, G. L. *Biochemistry* **2000**, *39*, 13760.

(12) Mims, W. B.; Peisach, J. *J. Chem. Phys.* **1978**, *69*, 4921.

(13) Jun, S.; Becker, J. S.; Yonkunas, M.; Coalson, R.; Saxena, S. *Biochemistry* **2006**, *45*, 11666.

Full references in the main text for (68) Gaussian 09 and (74) AMBER12:

(68) Frisch, M. J.; Trucks, G. W.; Schlegel, H. B.; Scuseria, G. E.; Robb, M. A.; Cheeseman, J. R.; Scalmani, G.; Barone, V.; Mennucci, B.; Petersson, G. A.; Nakatsuji, H.; Caricato, M.; Li, X.; Hratchian, H. P.; Izmaylov, A. F.; Bloino, J.; Zheng, G.; Sonnenberg, J. L.; Hada, M.; Ehara, M.; Toyota, K.; Fukuda, R.; Hasegawa, J.; Ishida, M.; Nakajima, T.; Honda, Y.; Kitao, O.; Nakai, H.; Vreven, T.; Montgomery, J. A., Jr.; Peralta, J. E.; Ogliaro, F.; Bearpark, M.; Heyd, J. J.; Brothers, E.; Kudin, K. N.; Staroverov, V. N.; Kobayashi, R.; Normand, J.; Raghavachari, K.; Rendell, A.; Burant, J. C.; Iyengar, S. S.; Tomasi, J.; Cossi, M.; Rega, N.; Millam, J. M.; Klene, M.; Knox, J. E.; Cross, J. B.; Bakken, V.; Adamo, C.; Jaramillo, J.; Gomperts, R.; Stratmann, R. E.; Yazyev, O.; Austin, A. J.; Cammi, R.; Pomelli, C.; Ochterski, J. W.; Martin, R. L.; Morokuma, K.; Zakrzewski, V. G.; Voth, G. A.; Salvador, P.; Dannenberg, J. J.; Dapprich, S.; Daniels, A. D.; Farkas, Ö.; Foresman, J. B.; Ortiz, J. V.; Cioslowski, J.; Fox, D. J. *Gaussian 09, Revision C.01*, Gaussian, Inc., Wallingford CT, 2009.

(74) Case, D. A.; Darden, T. A.; Cheatham, I., T.E ; Simmerling, C. L.; Wang, J.; Duke, R. E.; Luo, R.; Walker, R. C.; Zhang, W.; Merz, K. M. J.; Roberts, B.; Hayik, S.; Roitberg, A.; Seabra, G.; Swails, J.; Gotz, A. W.; Kolossvary, I.; Wong, K. F.; Paesani, F.; Vanicek, J.; Wolf, R. M.; Liu, J.; Wu, X.; Brozell, S.; Steinbrecher, H.; Gohlke, H.; Cai, Q.; Ye, X.; Wang, J.; Hsieh, M.-J.; Cui, G.; Roe, D. R.; Mathews, D. H.; Seetin, M. G.; Salomon-Ferrer, R.; Sagui, C.; Babin, V.; Luchko, T.; Gusarov, S.; Kovalenko, A.; Kollman, P. A. *AMBER 12*, University of California, San Francisco, CA, 2012.